

# LegoPET: Hierarchical Feature Guided Conditional Diffusion for PET Image Reconstruction

Yiran Sun  
Rice University  
6100 Main St, Houston, TX 77005  
ys92@rice.edu

Osama Mawlawi  
The University of Texas MD Anderson Cancer Center  
1155 Pressler St, Houston, TX 77030  
omawlawi@mdanderson.org

## Abstract

Positron emission tomography (PET) is widely utilized for cancer detection due to its ability to visualize functional and biological processes in vivo. PET images are usually reconstructed from histogrammed raw data (sinograms) using traditional iterative techniques (e.g., OSEM, MLEM). Recently, deep learning (DL) methods have shown promise by directly mapping raw sinogram data to PET images. However, DL approaches that are regression-based or GAN-based often produce overly smoothed images or introduce various artifacts respectively. Image-conditioned diffusion probabilistic models (cDPMs) are another class of likelihood-based DL techniques capable of generating highly realistic and controllable images. While cDPMs have notable strengths, they still face challenges such as maintain correspondence and consistency between input and output images when they are from different domains (e.g., sinogram vs. image domain) as well as slow convergence rates. To address these limitations, we introduce LegoPET, a hierarchical feature guided conditional diffusion model for high-perceptual quality PET image reconstruction from sinograms. We conducted several experiments demonstrating that LegoPET not only improves the performance of cDPMs but also surpasses recent DL-based PET image reconstruction techniques in terms of visual quality and pixel-level PSNR/SSIM metrics. Our code is available at <https://github.com/yiransun/LegoPET>.

## 1. Introduction

Positron emission tomography (PET) is a functional imaging technique that visualizes various biochemical and physiological processes across different tissues. During the image acquisition process, high-energy photons generated by positron annihilation are detected and counted by detectors arranged in rings within a PET scanner. Usually, the measured counts from various angles form projections,

which are then stacked into sinograms. These sinograms serve as the basis for reconstructing the final PET image, enabling the visualization of functional processes within the body [2].

Conventional PET image reconstruction techniques, such as Ordered Subsets Expectation Maximization (OSEM) and Maximum Likelihood Expectation Maximization (MLEM), often encounter challenges like data-model mismatch, data inconsistency, and overfitting, which may introduce artifacts and noise into the reconstructed images [4]. Recently, deep learning (DL) methods that directly transform raw PET sinograms into images have gained attention due to their ability to learn complex, non-linear physical processes from data. However, regression-based DL approaches are typically supervised with mean square error (MSE) or mean absolute error (MAE), leading to resultant images with overly smooth textures and suboptimal perceptual quality [11, 15]. Generative models, such as generative adversarial networks (GANs) [3], represent an advanced class of DL techniques designed to capture inherent data distributions and generate realistic images. Nevertheless, the underlying competitive nature between generator and discriminator segments of GAN models often leads to issues such as non-convergence and mode collapse during training [17]. Image-conditioned diffusion probabilistic models (cDPMs) [7, 8, 16] have lately demonstrated competitive performance, which exhibits better convergence behavior and generates more realistic images. However, cDPMs also face several key challenges: (1) insufficient correspondence and consistency between conditioning inputs and outputs, especially when they originate from different domains (e.g., sinogram vs. image domains), (2) difficulty in capturing high frequency details, and (3) low training efficiency [5, 19].

To address above limitations, we propose LegoPET, a hierarchical feature guided conditional diffusion model for high-perceptual quality PET image reconstruction from sinograms. Specifically, building on previous work [15, 18, 20], we first train a convolutional U-Net on sinogram-

PET pairs as a plug-and-play prior (PnPNet), and then efficiently fine-tune a standard cDPM by using structured multilevel features from the learned PnPNet as biases. Additionally, we use the classifier-free training strategy to balance mode coverage and sample fidelity [8]. Experimental results demonstrate that LegoPET not only improves the performance of cDPMs but also surpasses recent DL-based PET image reconstruction techniques in terms of visual quality and pixel-level PSNR/SSIM metrics.

## 2. Method

Let  $s$  denote input sinogram image, where  $s \in \mathbb{R}^{1 \times H \times W}$  is a single-channel 2D image with resolution  $H \times W$ . We denote the reference PET scan by  $\mathbf{x}_0 \in \mathbb{R}^{1 \times H \times W}$ . Our general objective is to approximate and sample from the conditional distribution  $p(\mathbf{x}_0|s)$ . We develop LegoPET to address this task, containing two components (see Fig. 1): a learned plug-and-play prior network (right) that generates hierarchical feature maps, and a standard 2D sinogram-conditioned diffusion model (left) that reconstructs final clean PET image. We describe details of LegoPET in the following sections.

### 2.1. Plug-and-Play Prior Network (PnPNet)

We utilize a conditional convolutional U-Net, which is the same architecture as commonly-used U-Net backbone in diffusion models, consisting of ResNet blocks [6] and spatial self-attention blocks. Specifically, PnPNet comprises 4 encoder blocks, 2 middle blocks, and 4 decoder blocks, taking a single sinogram  $s$  as input and getting the corresponding PET image information (see Fig. 1b). In our experiments, input and output have been padded with dimensions of  $1 \times 256 \times 256$ . During downsampling stage, the blocks operate at 4 resolutions:  $256 \times 256$ ,  $128 \times 128$ ,  $64 \times 64$ ,  $32 \times 32$ . Note that PnPNet’s architecture is not limited to this design and may perform similarly well with other architectural variations.

PnPNet is trained in an end-to-end manner using spatial MSE-based ( $\mathcal{L}_{MSE}$ ) and Discrete Wavelet Transform-based ( $\mathcal{L}_{DWT}$ ) [13] losses for supervision on sinogram-PET pairs:

$$\mathcal{L}_{\text{PnPNet}} = \mathcal{L}_{MSE} + \lambda_1 * \mathcal{L}_{DWT} \quad (1)$$

where  $\lambda_1$  controls the importance of DWT loss term (we set  $\lambda_1 = 0.1$  in our experiments).  $\mathcal{L}_{DWT}$  mainly focuses on calculating the difference between ground truth and prediction’s high-frequency spectrum, which ensures that the hierarchical feature maps from PnPNet are able to additionally capture more high-frequency information (e.g. tissue edges, anatomical structures, textures).

Then we extract two lists of hierarchical feature maps from downsampling blocks ( $b_d$ ) and middle blocks ( $b_m$ ) in

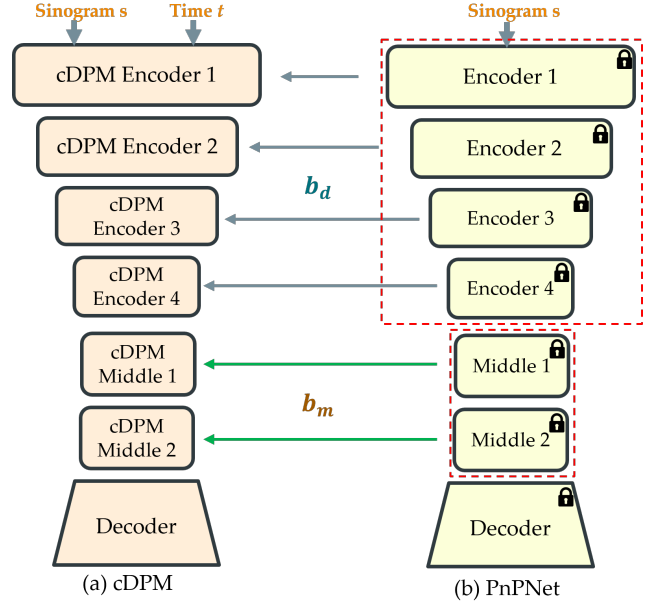


Figure 1. **Overview of LegoPET.** LegoPET includes two parts: a learned PnPNet for hierarchical feature maps extraction (right), and a standard 2D sinogram-conditioned DPM for PET image reconstruction (left). Two lists of structured layered feature maps,  $b_d$  and  $b_m$ , from the pre-trained PnPNet are added to the cDPM as biases.

the latent space of learned PnPNet. We connect the pre-trained PnPNet to cDPM by incorporating  $b_d$  and  $b_m$  as extra biases to the encoder and middle blocks of cDPM. This integration allows the cDPM to leverage the low- and high-frequency information from learned feature representations.

### 2.2. LegoPET for Sinogram-to-PET

Conditional DPMs (cDPMs) are designed to learn a parameterized Markov chain that transforms a Gaussian distribution into a conditional data distribution. In particular, LegoPET approximates the conditional distribution through a fixed forward process and a learning-based reverse process.

The forward process starts with a clean PET sample from the input data distribution  $\mathbf{x}_0 \sim q(\mathbf{x}_0)$  and gradually adds Gaussian noise according to a variance schedule  $\beta_{1:T}$ , where  $\beta_t \in (0, 1)$  for all  $t \in [1, T]$ :

$$q(\mathbf{x}_t|\mathbf{x}_{t-1}) := \mathcal{N}(\mathbf{x}_t; \sqrt{1 - \beta_t}\mathbf{x}_{t-1}, \beta_t\mathbf{I}) \quad (2)$$

where  $\mathbf{x}_T$  is an isotropic Gaussian distribution for large enough  $T$ . We express  $\mathbf{x}_t$  in closed form with respect to  $\mathbf{x}_0$  directly, which allows for efficient training. Let  $\alpha_t := 1 - \beta_t$ ,  $\bar{\alpha}_t := \prod_{s=1}^t \alpha_s$ . Then we can sample  $\mathbf{x}_t$  at any time step  $t$  using a linear combination of noise  $\epsilon \sim \mathcal{N}(0, \mathbf{I})$  and  $\mathbf{x}_0$ :

$$\mathbf{x}_t = \sqrt{\bar{\alpha}_t}\mathbf{x}_0 + \sqrt{1 - \bar{\alpha}_t}\epsilon \quad (3)$$

The goal of reverse process is to generate a clean PET image  $\mathbf{x}_0$  from the noisy vector  $\mathbf{x}_T$  given the conditions  $\mathcal{C} = \{s, b_d, b_m\}$ , i.e. approximate specific conditional distribution  $p(\mathbf{x}_0|\mathcal{C})$ . We use a joint Markov chain distribution to model this process:  $p_\theta(\mathbf{x}_{0:T}) := p(\mathbf{x}_T) \prod_{t=1}^T p_\theta(\mathbf{x}_{t-1}|\mathbf{x}_t, \mathcal{C})$ , where  $p(\mathbf{x}_T) = \mathcal{N}(\mathbf{x}_T; \mathbf{0}, \mathbf{I})$ . We learn the transition  $p_\theta(\mathbf{x}_{t-1}|\mathbf{x}_t, \mathcal{C})$  using a neural network  $\mu_\theta(\cdot, \cdot)$ :

$$p_\theta(\mathbf{x}_{t-1}|\mathbf{x}_t, \mathcal{C}) := \mathcal{N}(\mathbf{x}_{t-1}; \mu_\theta(\mathbf{x}_t, t, \mathcal{C}), \Sigma_\theta(\mathbf{x}_t, t, \mathcal{C})) \quad (4)$$

where  $\theta$  represents the learnable parameters of the neural network. We can further reparameterize  $\mu_\theta(\cdot, \cdot)$  by:

$$\mu_\theta(\mathbf{x}_t, t, \mathcal{C}) = \frac{1}{\sqrt{\alpha_t}} \left( \mathbf{x}_t - \frac{1 - \alpha_t}{\sqrt{1 - \bar{\alpha}_t}} \epsilon_\theta(\mathbf{x}_t, t, \mathcal{C}) \right) \quad (5)$$

where  $\epsilon_\theta(\cdot, \cdot)$  predicts the noise added at each time step.

### 2.3. Training and Inference

Following previous diffusion model-based work, we use a time-conditioned convolutional U-Net to perform denoising at each time step of the reverse process. We incorporate conditions  $\mathcal{C}$  into the denoising process. During each iteration of training, a batch of random sinogram-PET pairs is selected, and LegoPET is trained by minimizing the denoising loss:

$$\mathcal{L}_{\text{LegoPET}} := \mathbb{E}_{t \sim [1, T], \mathbf{x}_0, \epsilon} [ \|\epsilon_t - \epsilon_\theta(\mathbf{x}_t, t, \mathcal{C})\|^2 ] \quad (6)$$

We use classifier-free diffusion guidance training strategy. The conditioning information  $\mathcal{C}$  is randomly removed with probability  $p_{dp}$  and replaced with the same shape null tensors representing the absence of conditioning information. This strategy assists LegoPET to effectively capture both conditional and unconditional distributions, also the differences between them, thereby generating results that are more accurately aligned with the conditioning information [8].

At inference time, given a sample of Gaussian noise  $\mathbf{x}_T \sim \mathcal{N}(0, \mathbf{I})$ , we use new denoising expression  $\tilde{\epsilon}_\theta = (1 + \lambda_2)\epsilon_\theta(\mathbf{x}_t, t, \mathcal{C}) - \lambda_2\epsilon_\theta(\mathbf{x}_t, t)$  to progressively denoise  $\mathbf{x}_T$  over  $T$  steps to generate a clean PET image  $\mathbf{x}_0$ , where  $\lambda_2$  controls the relative importance of different terms.

## 3. Experiments

### 3.1. Datasets and Preprocessing

We simulated 2D  $^{18}\text{F}$ -FDG PET images using the public 20 3D brain phantoms from BrainWeb [1] with the resolution and matrix size of  $2.086 \times 2.086 \times 2.031 \text{ mm}^3$  and  $344 \times 344 \times 127$  acquired from a Siemens Biograph mMR. We used data augmentation technique by rotating each 3D brain phantom 5 times. For each 3D brain phantom, we

selected 55 non-continuous slices from axial view to generate high count sinograms which were used to reconstruct the reference PET images. We used 17 brain samples (4675 slices) for training, 1 brain sample (275 slices) for validation and 2 brain samples (550 slices) for testing.

### 3.2. Implementation Details

We implemented all experiments using PyTorch [14] on NVIDIA A100 GPUs. We trained PnPNet using the Adam optimizer with a fixed learning rate of  $3 \times 10^{-5}$ , and selected the model at epoch 119. We set batch size to 4 and trained 500 epochs for each LegoPET model, with  $T = 1000$  timesteps and  $p_{dp} = \{0, 0.1, 0.2, 0.5\}$ . We chose the final checkpoints for all LegoPETs without any specific selection strategies. We used pixel-level metrics for quantitative evaluation, i.e. Peak Signal to Noise Ratio (PSNR) and Structural Similarity Index Measure (SSIM) [9]. Our code is available at <https://github.com/yransun/LegoPET>.

### 3.3. Baselines

We compared LegoPET against four baselines: DeepPET [4], cGAN [12], Pix2Pix [10] and cDPM [8, 16]. DeepPET is a regression-based method that utilizes a deep convolutional encoder-decoder network to map sinograms directly to PET images. cGAN is a standard conditional GAN for image reconstruction. Pix2Pix uses a conditional least squares GAN for image-to-image translation tasks. cDPM is a standard sinogram-conditioned diffusion model, which can also be regarded as “*LegoPET w/o guidance*”. We used the publicly provided repository configurations for all baseline models and trained them until full convergence.

### 3.4. Reconstruction Results

We summarize the average pixel-wise PSNR/SSIM values across all reconstructed slices and the number of trainable parameters for each method in Table 1. LegoPET demonstrates a 0.59dB improvement in PSNR compared to cDPM, validating the effectiveness of the proposed hierarchical feature-guided module. Additionally, we observe a substantial improvement of approximately 5dB/3.7dB in PSNR when compared with cGAN/Pix2Pix. Although DeepPET achieves comparable PSNR values to LegoPET, the PET images reconstructed by DeepPET are significantly less aligned with human visual perception, as shown in Fig. 2. This may be due to LegoPET’s reliance on diffusion-based generative models and stochastic posterior sampling, which compromises pixel-wise distortion (leading to lower PSNR) while maintaining fidelity to the target image [11, 15]. Visual reconstruction results are further illustrated in Fig. 2, with side-by-side comparisons of four baseline methods. LegoPET generates the most realistic reconstruction results among all methods, with the second lightest color in the squared error maps. cGAN, Pix2Pix,

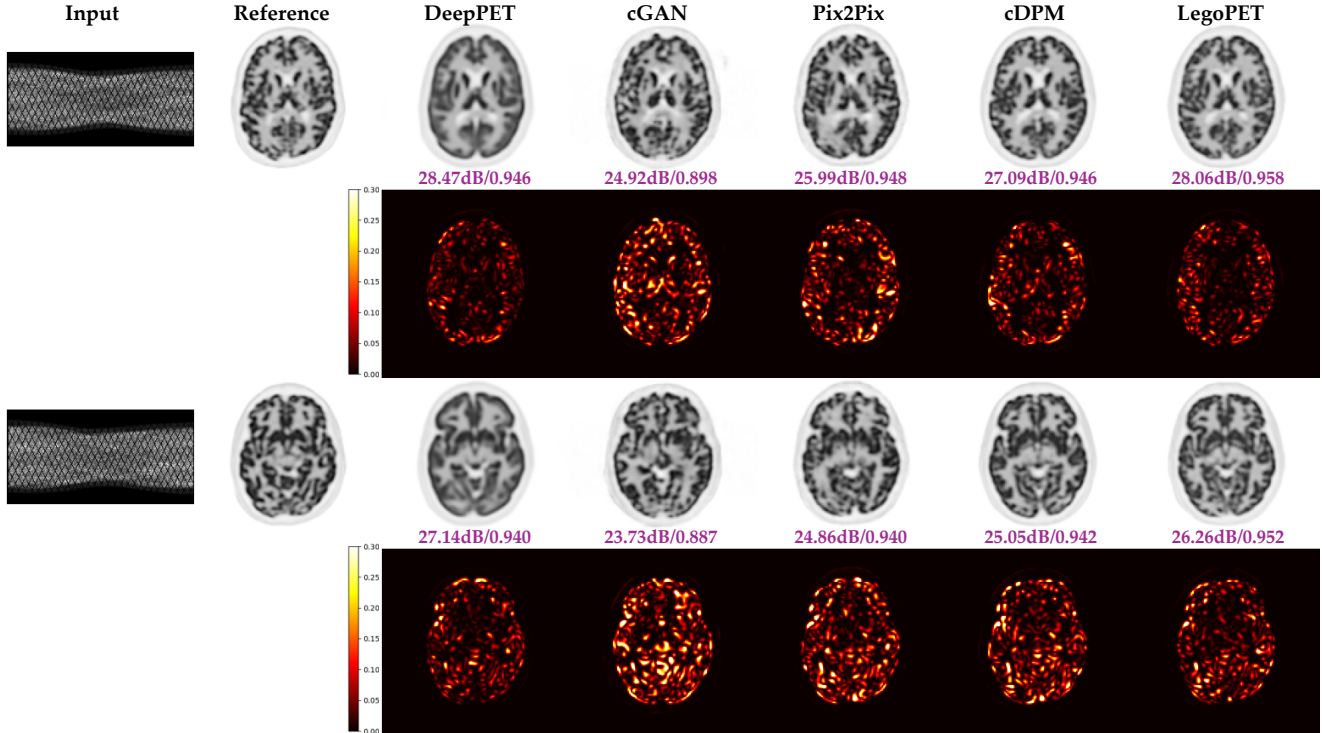


Figure 2. **Comparison of LegoPET with Four Baselines on Two Example Reconstructed Slices.** The first column shows the input sinogram images, and the second column shows the reference images reconstructed using OSEM algorithm. The third to sixth columns correspond to the four baselines (labeled above each image), and the final column shows the reconstructed PET image using proposed LegoPET method. PSNR/SSIM values are reported below each slice, and squared error maps between each method and the reference image are also displayed (second and fourth rows). We prove that LegoPET generates PET images with the highest perceptual quality, and also improves the performance of cDPM through feature guidance.

Category	Method	Metrics		
		PSNR $\uparrow$	SSIM $\uparrow$	MParam.
Regression-based	DeepPET [4]	<b>28.30</b>	0.944	11.02
GAN-based	cGAN [12]	22.58	0.864	11.37
	Pix2Pix [10]	23.91	0.922	11.37
Likelihood-based	cDPM [8]	27.00	<b>0.945</b>	35.71
	<b>LegoPET (Ours)</b>	<b>27.59</b>	<b>0.956</b>	35.71

Table 1. **Quantitative Evaluation using PSNR, SSIM, and Number of Trainable Parameters (MParam).** Red and blue colors indicate the best and second-best results respectively.

and cDPM introduce numerous artifacts, while DeepPET produces blurry reconstructions with unrealistic fine details.

### 3.5. Ablation Study

To further verify the effectiveness of our proposed LegoPET, we conducted an ablation study. For a fair comparison, we used the same training settings for both cDPM and LegoPET, including learning rate and the number of trainable parameters. Classifier-free diffusion guidance [8] was disabled during the ablation study, i.e.  $p_{dp} = 0$ . We

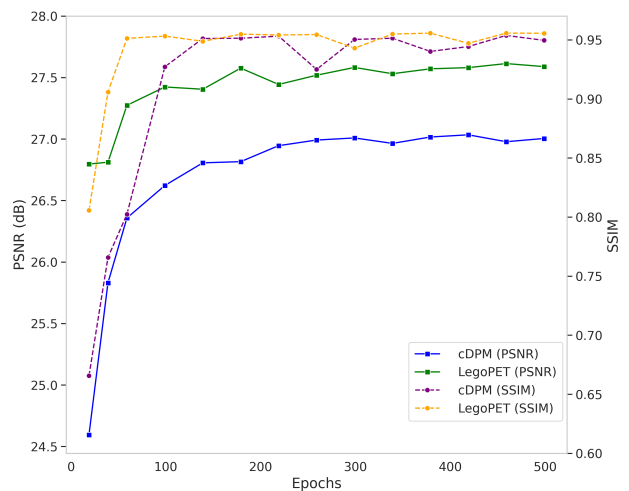


Figure 3. **Effectiveness of Hierarchical Feature Guidance.** We compare the performance of LegoPET and cDPM within 500 epochs in terms of PSNR and SSIM. We regard cDPM as “LegoPET w/o guidance”, and LegoPET as “cDPM w/ guidance”.

compared their performance every 20 epochs in terms of PSNR/SSIM over a total of 500 epochs. The results presented in Fig. 3 reveal several key insights as expected. First, LegoPET consistently outperforms cDPM in terms of quantitative metrics, which underscores the benefits of integrating hierarchical feature representations with rich low- and high-frequency information from learned PnPNet into a cDPM. Second, LegoPET illustrates strong performance even at early epochs, suggesting its potential to improve training efficiency.

## 4. Conclusion

We propose LegoPET, which enables high-perceptual quality PET image reconstruction that preserves geometric structure and sharp edges from raw sinograms. The experimental results show that LegoPET outperforms several baseline algorithms in terms of visual inspection and PSNR/SSIM metrics. The ablation study further validates that our novel hierarchical feature-guided method has significant potential to improve both reconstructed image quality and training efficiency. Our future work will focus on extending current model into an efficient 3D version and validating on patient data.

## References

- [1] D Louis Collins, Alex P Zijdenbos, Vasken Kollokian, John G Sled, Noor Jehan Kabani, Colin J Holmes, and Alan C Evans. Design and construction of a realistic digital brain phantom. *IEEE transactions on medical imaging*, 17(3):463–468, 1998. [3](#)
- [2] Frederic H Fahey. Data acquisition in pet imaging. *Journal of nuclear medicine technology*, 30(2):39–49, 2002. [1](#)
- [3] Ian Goodfellow, Jean Pouget-Abadie, Mehdi Mirza, Bing Xu, David Warde-Farley, Sherjil Ozair, Aaron Courville, and Yoshua Bengio. Generative adversarial networks. *Communications of the ACM*, 63(11):139–144, 2020. [1](#)
- [4] Ida Häggström, C Ross Schmidlein, Gabriele Campanella, and Thomas J Fuchs. Deeppet: A deep encoder–decoder network for directly solving the pet image reconstruction inverse problem. *Medical image analysis*, 54:253–262, 2019. [1](#), [3](#), [4](#)
- [5] Zeyu Han, Yuhan Wang, Luping Zhou, Peng Wang, Binyu Yan, Jiliu Zhou, Yan Wang, and Dinggang Shen. Contrastive diffusion model with auxiliary guidance for coarse-to-fine pet reconstruction. In *International Conference on Medical Image Computing and Computer-Assisted Intervention*, pages 239–249. Springer, 2023. [1](#)
- [6] Kaiming He, Xiangyu Zhang, Shaoqing Ren, and Jian Sun. Deep residual learning for image recognition. In *Proceedings of the IEEE conference on computer vision and pattern recognition*, pages 770–778, 2016. [2](#)
- [7] Jonathan Ho, Ajay Jain, and Pieter Abbeel. Denoising diffusion probabilistic models. *Advances in neural information processing systems*, 33:6840–6851, 2020. [1](#)
- [8] Jonathan Ho and Tim Salimans. Classifier-free diffusion guidance. *arXiv preprint arXiv:2207.12598*, 2022. [1](#), [2](#), [3](#), [4](#)
- [9] Alain Hore and Djemel Ziou. Image quality metrics: Psnr vs. ssim. In *2010 20th international conference on pattern recognition*, pages 2366–2369. IEEE, 2010. [3](#)
- [10] Phillip Isola, Jun-Yan Zhu, Tinghui Zhou, and Alexei A Efros. Image-to-image translation with conditional adversarial networks. In *Proceedings of the IEEE conference on computer vision and pattern recognition*, pages 1125–1134, 2017. [3](#), [4](#)
- [11] Christian Ledig, Lucas Theis, Ferenc Huszár, Jose Caballero, Andrew Cunningham, Alejandro Acosta, Andrew Aitken, Alykhan Tejani, Johannes Totz, Zehan Wang, et al. Photorealistic single image super-resolution using a generative adversarial network. In *Proceedings of the IEEE conference on computer vision and pattern recognition*, pages 4681–4690, 2017. [1](#), [3](#)
- [12] Mehdi Mirza and Simon Osindero. Conditional generative adversarial nets. *arXiv preprint arXiv:1411.1784*, 2014. [3](#), [4](#)
- [13] Gheyath Othman and Diyar Qader Zeebaree. The applications of discrete wavelet transform in image processing: A review. *Journal of Soft Computing and Data Mining*, 1(2):31–43, 2020. [2](#)
- [14] Adam Paszke, Sam Gross, Francisco Massa, Adam Lerer, James Bradbury, Gregory Chanan, Trevor Killeen, Zeming Lin, Natalia Gimelshein, Luca Antiga, et al. Pytorch: An imperative style, high-performance deep learning library. *Advances in neural information processing systems*, 32, 2019. [3](#)
- [15] Mengwei Ren, Mauricio Delbracio, Hossein Talebi, Guido Gerig, and Peyman Milanfar. Multiscale structure guided diffusion for image deblurring. In *Proceedings of the IEEE/CVF International Conference on Computer Vision*, pages 10721–10733, 2023. [1](#), [3](#)
- [16] Chitwan Saharia, William Chan, Huiwen Chang, Chris Lee, Jonathan Ho, Tim Salimans, David Fleet, and Mohammad Norouzi. Palette: Image-to-image diffusion models. In *ACM SIGGRAPH 2022 conference proceedings*, pages 1–10, 2022. [1](#), [3](#)
- [17] Tim Salimans, Ian Goodfellow, Wojciech Zaremba, Vicki Cheung, Alec Radford, and Xi Chen. Improved techniques for training gans. *Advances in neural information processing systems*, 29, 2016. [1](#)
- [18] Yiran Sun and Osama R Mawlawi. Diffpet: A fine tuned sinogram-to-pet conditional diffusion model. In *AAPM 66th Annual Meeting & Exhibition*. AAPM, 2024. [1](#)
- [19] Huijie Zhang, Yifu Lu, Ismail Alkhouri, Saiprasad Ravishankar, Dogyoon Song, and Qing Qu. Improving training efficiency of diffusion models via multi-stage framework and tailored multi-decoder architecture. In *Proceedings of the IEEE/CVF Conference on Computer Vision and Pattern Recognition*, pages 7372–7381, 2024. [1](#)
- [20] Lvmin Zhang, Anyi Rao, and Maneesh Agrawala. Adding conditional control to text-to-image diffusion models. In *Proceedings of the IEEE/CVF International Conference on Computer Vision*, pages 3836–3847, 2023. [1](#)